X-RAY EMISSION MECHANISMS IN PROTOSTELLAR JETS

R. Bonito[1], S. Orlando[2], G. Peres[1], F. Favata[3] and R. Rosner[4,5]

[1]Dip. Scienze Fisiche ed Astronomiche, Sez. Astronomia, Università di Palermo, P.zza del Parlamento 1, 90134 Palermo, Italy
[2]INAF – Osservatorio Astronomico di Palermo, P.zza del Parlamento 1, 90134 Palermo, Italy
[3]Astrophysics Div. – Research and Space Science Dept. ESA, ESTEC, Postbus 299, NL-2200 AG Noordwijk, The Netherlands
[4]Dept. of Astronomy and Astrophysics, Univ. of Chicago, Chicago, IL 60637
[5]Center for Astrophysical Thermonuclear Flashes, University of Chicago, 5640 S. Ellis Avenue, Chicago, IL 60637, USA

Abstract

Prompted by the recent detection of X-ray emission from Herbig-Haro objects, we studied the interaction between a supersonic jet originating from a young stellar object and the ambient medium; our aim is to investigate the mechanisms causing the X-ray emission. Our model takes into account the radiative losses from optically thin plasmas and Spitzer's thermal conduction including saturation effects. We explored the parameter space defined by the density contrast between the ambient medium and the jet and by the Mach number, to infer the configurations which can give rise to X-ray emission. From the models, we derived the X-ray emission as it would be observed with *Chandra*/ACIS-I and XMM-*Newton*/EPIC-pn, using the MEKAL spectral code and including the absorption of interstellar medium. Here we discuss a representative case which produces, without any ad hoc assumption, X-ray emission with characteristics very similar to those observed in the protostellar jet, HH 154. We find that the X-ray emission originates from a blob localized just behind the bow shock, moving with velocity 500 km/s. We predict, therefore, among other features, a detectable proper motion of the X-ray blob, which is interesting for future observations.

Key words: ISM: Herbig-Haro objects – ISM: individual objects (HH 154) – ISM: jets and outflows – X-rays: ISM

1. Introduction

Herbig-Haro objects are mainly shocks produced at the interaction front between the supersonic protostellar jet and the ambient medium. Optical, radio and infrared studies of these objects have been carried since HH objects were discovered (Herbig 1950; Haro 1953). Recently X-ray emission with the XMM-*Newton* and *Chandra* satellites has been detected for a few of these HH objects: HH 2 in Orion (Pravdo et al. 2001), HH 154 in Taurus (Favata et al. 2002; Bally et al. 2003), HH 80/81 in the Sagittarius cloud L291 (Pravdo et al. 2004), and a protostellar jet in the OMC-3 molecular cloud in Orion (Tsujimoto et al. 2004).

As an example the left panel of the Fig. 1 shows an optical image of the protostellar jet HH 154 located at the distance of 140 pc in Taurus (adapted from Bally et al. 2003). This figure shows the position of the X-ray source marked with a cross at the base of the jet.

The right panel of Fig. 1 is a close up view of the X-ray source detected with *Chandra*/ACIS-I (Bally et al. 2003). The X-ray source is not coincident with the position of the protostar. The protostar suffers a visual extinction of $\sim$ 150 mag whereas a small visual extinction of ~ 7 mag has been found for the soft X-ray source, with a temperature of a few million degrees. This makes HH 154 an ideal object to be studied because the emission from the protostar is obscured.

Prompted by these new observations we started a project devoted to study the mechanism causing the X-ray emission detected in HH objects. This work is part of a wider project in which we perform a detailed exploration of the parameter space and we take into account all the important physical effects describing the evolution of a protostellar jet.

In this paper we study the X-ray emission from HH 154, the nearest and one of the best studied Herbig-Haro objects emitting X-rays. X-ray emission from HH 154 has been detected with both XMM-*Newton* and *Chandra* (Favata et al. 2002; Bally et al. 2003). The aim of our work is to infer the configuration which can give rise to X-ray emission, to derive detailed predictions, to determine the range of parameters consistent with observations and to get insight on the jet physical conditions. To this end we performed a detailed modeling of the interaction between a supersonic plasma jet and a uniform ambient medium using the FLASH code (Fryxell et al. 2000). FLASH is an accurate and very advanced numerical code which uses the PARAMESH library to handle adaptive mesh refinement (MacNeice et al. 2000). The code uses the Message Passing Interface (MPI) library to achieve parallelization. For our simulations FLASH included modules that treat optically thin radiative losses and thermal conduction.

The paper is structured as follows: Sect. 2 describes the proto-stellar jet model; Sect. 3 describes our method to synthesize, from the numerical simulations, X-ray observations as predicted to be observed with *Chandra* and XMM-*Newton*; in Sect. 4 we discuss the results of the numerical simulations; finally in Sect. 5 we draw our conclusions.

Proc. 13th Cool Stars Workshop, Hamburg, 5–9 July 2004 (ESA SP-560, Jan. 2005, F. Favata, G. Hussain & B. Battrick eds.)

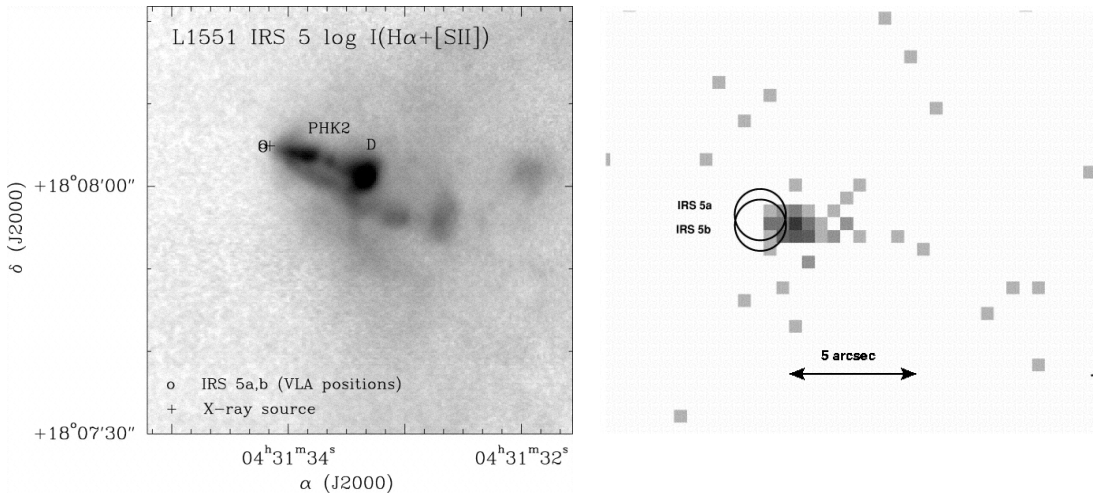

Figure 1. Left panel: an optical image of the protostellar jet HH 154 (adapted from Bally et al. 2003). The location of the X-ray source detected with Chandra *is marked with a cross. The two circles mark the position of the binary system IRS* 5 *from which the jet originates. Right panel: close-up view of the X-ray source associated with HH 154 (Bally et al. 2003). The circles correspond to the position of the binary protostar IRS 5.*

2. The model

The evolution of the protostellar jet traveling through the ambient medium is described by the fluid equations of mass, momentum and energy conservation in the form

$$\frac{\partial \rho}{\partial t} + \nabla \cdot \rho \mathbf{v} = 0 \tag{1}$$

$$\frac{\partial \rho \mathbf{v}}{\partial t} + \nabla \cdot \rho \mathbf{v}\mathbf{v} + \nabla p = 0 \tag{2}$$

$$\frac{\partial \rho E}{\partial t} + \nabla \cdot (\rho E + p)\mathbf{v} = -\nabla \cdot q - n_e n_{\rm H} P(T) \tag{3}$$

where t is the time, ρ is the mass density, v is the plasma velocity, q is the conductive flux, n_e and $n_{\rm H}$ are the electron and hydrogen density respectively, $P(T)$ indicates the radiative losses per unit emission measure. In our model we assume a negligible magnetic field and we take into account optically thin radiative losses (Raymond & Smith 1977 and subsequent upgrades; Mewe et al. 1985) and thermal conduction in the form (Dalton & Balbus 1993)

$$q = \left(\frac{1}{q_{\rm spi}} + \frac{1}{q_{\rm sat}} \right)^{-1} \tag{4}$$

where

$$q_{\rm spi} = -k_s T^{5/2} \nabla T \tag{5}$$

where k_s is almost constant, T is the plasma temperature, in the Spitzer regime (Spitzer 1962) and

$$q_{\rm sat} = -sign(\nabla T) 5 \phi \rho c_s^3 \tag{6}$$

where $\phi \sim 1.1$ and c_s is the sound speed, with saturation effects (Cowie & McKee 1977) taken into account.

We adopt a bi-dimensional cylindrical coordinate system with the jet axis coincident with the z axis. The computational grid extends over 300 AU in the radial direction and over 6500 AU in the z direction. Reflection boundary conditions are imposed along the jet axis, inflow boundary conditions at $z = 0$ and $r \leq r_{\rm j}$, $r_{\rm j}$ being the initial jet radius, and outflow boundary conditions elsewhere. We assumed that at the beginning the jet is in pressure equilibrium with its environment. The initial jet radius is 30 AU and its initial length is 300 AU. The initial jet velocity is along the z axis, coincident with the jet axis, and is a function of the distance from the axis, r, as follow

$$V(r) = \frac{V_0}{\nu \cosh(r/r_{\rm j})^w - (\nu - 1)} \tag{7}$$

where V_0 is the on-axis velocity, ν is the ambient to jet density ratio, $r_{\rm j}$ is the initial jet radius and w is the steepness parameter for the shear layer (in all the simulations we assumed $w = 4$). The change of the density in the radial direction is

$$\rho = \rho_{\rm j} \left(\nu - \frac{\nu - 1}{\cosh(r/r_{\rm j})^w} \right) \tag{8}$$

where $\rho_{\rm j}$ is the jet density.

The maximum spatial resolution achieved in our simulations is 1.3 AU, using 4 refinement levels according to the

PARAMESH methodology. This resolution corresponds to covering the jet radius with 25 mesh points.

3. Synthesizing the X-ray spectra

From the model we derive the emission measure, EM, and the temperature, T, for each fluid element, and we obtain 3-D maps of EM and T, considering the axial symmetry. From these 3-D maps we derive the X-ray emission map integrating along the line of sight and taking into account the interstellar absorbing column density, $N_{\rm H} \approx 1.4 \times 10^{22}$ cm^{-2} as in Favata et al. (2002), and the *Chandra*/ACIS-I instrumental response. Following Orlando et al. (2000), we derive a distribution of emission measure vs. temperature, $EM(T)$, over the temperature range $10^3 - 10^8$ K. For this purpose we divide the temperature range into 74 bins, equispaced on a logarithmic scale; then the emission measure of all the elements corresponding to the same temperature bin is summed to yield the EM in that bin. From the $EM(T)$ distribution we synthesize the spectrum using the MEKAL spectral code (Mewe et al. 1985) taking into account the interstellar medium absorption column density, $N_{\rm H}$ (Morrison & McCammon 1983). Folding this absorbed parent spectrum through the instrument spectral response, we derive the focal plane spectrum as they would be detected with the *Chandra*/ACIS-I or XMM-*Newton*/EPIC-pn X-ray imaging spectrometers. We then analyze synthesized focal plane spectra with standard analysis tools (XSPEC V11.2), comparing our results with observations (Favata et al. 2002).

4. Results

Our model solutions depend on several physical parameters: the jet and ambient temperature and density, and the jet velocity. In order to reduce the number of free parameters, we assumed the initial jet temperature and density according to observations; in particular we assumed jet density[1], $n_{\rm j} = 500$ cm^{-3}, and jet temperature $T_{\rm j} = 10^4$ K as in Fridlund & Liseau (1998) and Favata et al. (2002). Our model solutions therefore are defined by the following free parameters: the Mach number, $M = v_{\rm j}/c_{\rm a}$ and the ambient to jet density ratio, $\nu = n_{\rm a}/n_{\rm j}$. In a forthcoming paper (Bonito et al. 2005) we discuss the results obtained from a wide exploration of the parameters space, (N, ν). From such an exploration we derived that only for a narrow range of values the parameters reproduce the observations. Here we present the model which shows the best agreement with observations of HH 154 (Bonito et al. 2004): a jet with Mach number $M = 300$, corresponding to an initial velocity $v_{\rm j} \approx 1400$ km s^{-1}, and with ambient-to-jet density contrast $\nu = n_{\rm a}/n_{\rm j} = 10$, corresponding to an ambient density, $n_{\rm a} = 5000$ cm^{-3}. Note that $\nu = 10$ corresponds to a jet less dense than the ambient medium, according to Fridlund & Liseau (1998). As shown in detail in Bonito et al. (2005) a jet traveling through a less dense ambient medium cannot reproduce results consistent with observations of HH 154, neither for the X-ray luminosity nor for the velocity observed.

Fig. 2 (upper panels) shows the evolution of the jet temperature (on the left) and density (on the right) both in a logarithmic grey scale. A cocoon with an almost uniform (because of the thermal conduction) temperature up to $T \approx 7 \times 10^5$ K envelops the jet. The cocoon temperature decreases in time and a cooler and denser shell forms.

In Fig. 3 we present an enlargement of the post shock region in a linear grey scale (temperature on the left and density on the right). A dense and hot blob with temperature of over 4×10^6 K and density $n_b \sim 10^4$ cm^{-3} is localized just behind the shock front.

Fig. 2 (lower panels) shows the predicted evolution of the X-ray emission, integrated along the line-of-sight with a bin size ~ 10 AU, as it would be observed with *Chandra*/ACIS-I. The *Chandra* resolution corresponds to ~ 60 AU at the distance of HH 154 (~ 140 pc). We found that the X-ray emission originates from the hot and dense blob localized just behind the shock front. Even with *Chandra* this blob cannot be spatially resolved and will be detected as a point-like source. Fig. 2 clearly shows a measurable proper motion for the X-ray blob. We found an average shock velocity $v_{\rm sh} \approx 500$ km s^{-1} corresponding to $\sim 0.7''$ yr^{-1}.

In order to compare our findings with observations, we synthesized the focal plane spectra as detected with EPIC-pn. From the 3-D maps of EM and T, we integrated the emission of the whole spatial domain. We assumed 10^2 total counts. We grouped the energy channels in order to have at least 10 photon counts per channel.

The evolution of the X-ray luminosity, $L_{\rm X}$ derived from our model in the EPIC band is shown in Fig. 4. We found that $L_{\rm X}$ varies moderately with time ranging between 2 and 5×10^{29} erg s^{-1}. These values are in good agreement with that obtained for HH 154, $L_{\rm X} = 3 \times 10^{29}$ erg s^{-1}, by Favata et al. (2002). The dashed line superimposed on Fig. 4 corresponds to $L_{\rm X}$ derived from the simple analytic model proposed by Raga et al. (2002). They assume that the X-ray emitting region is localized at the head of the bow shock, where the gas temperature and density are of the order of the on-axis post-shock values. Considering the radius of the blob $r_{\rm b} \approx 30$ AU, the ambient density, $n_{\rm a} \approx 5000$ cm^{-3}, and the shock velocity, $v_{\rm sh} \approx 500$ km s^{-1}, the model of Raga et al. (2002) predicts $L_{\rm X} = 2 \times 10^{29}$ erg s^{-1}. From Fig. 4 it is clear that our simulations confirm the prediction of Raga et al. (2002). In addition our model demonstrates that the X-ray source is effectively coincident with the blob localized just behind the shock front. Furthermore the good agreement between the analytic model proposed by Raga et al. (2002) and our simu-

[1] Note that density of 10^4 cm^{-3} corresponds to the shock front which generates the so-called knot D (Fig. 1); this is not the value of the jet density before it interacts with the ambient medium.

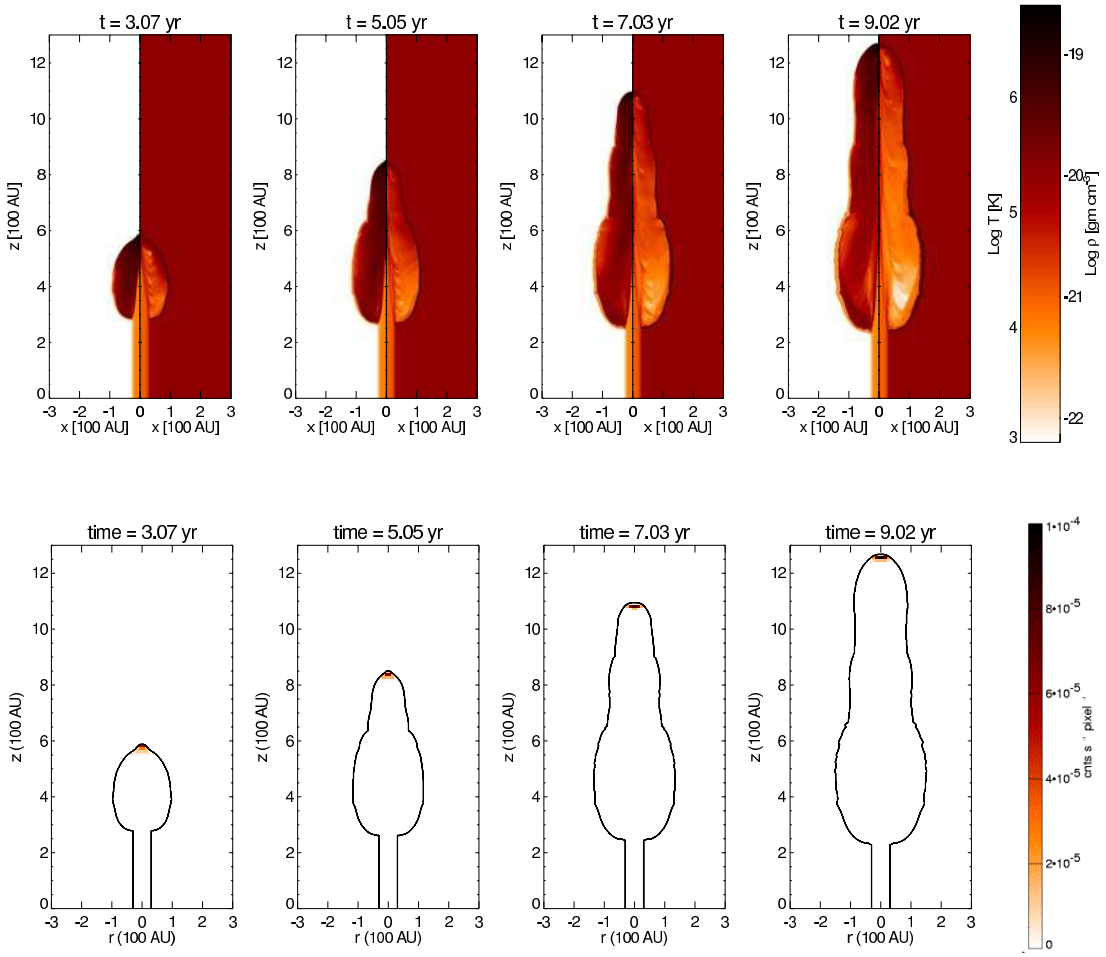

Figure 2. Upper panels: 2-D cuts through the rz plane of the jet temperature (on the left) and density (on the right) at four different evolutionary stages. Lower panels: X-ray emission integrated along the line-of-sight and on macro-pixels with ~ 10 AU size (6 times better that the ACIS-I spatial resolution), as we predict it would be observed with ACIS-I. The contour plot marks the region occupied by the jet and by the cocoon. The X-ray source is localized in a blob behind the bow shock, moving with measurable proper motion; its linear size is ~ 30 AU.

lations is based on the presence of a strong absorption due to the interstellar medium which suppresses the soft X-ray emission component originating from the cocoon with low temperature, $T \leq 10^6$ K.

As an example in Fig. 5 we present the synthesized spectrum 25 years since the beginning of the jet-ambient interaction, similar to Favata et al. (2002) observations. The MEKAL best-fit spectrum is also shown. Assuming a distance of about 150 pc we obtained 1.2 cnts ks^{-1} in the $[0.3-10]$ keV band with an absorbing column density of 1.5×10^{22} cm^{-2} (Tab. 1). All the spectra are well fitted with the emission from an optically thin plasma at a single temperature. The fitting parameters derived from our model (Tab. 1) are consistent with those obtained from the observations (Favata et al. 2002).

5. Discussion and conclusions

We have modeled the X-ray emission from protostellar jets. To this end we developed a fluid-dynamic model in which we have also taken into account optically thin radiative losses and thermal conduction effects. Using this model we performed an exploration of a wide parameters space and we found that the model yields observable X-ray emission only for plasma parameters close to the observed ones. As a result, we obtain a diagnostic power and insight on the physical configuration of a protostellar jet emitting X-ray. Our model predicts that the X-ray source origi-

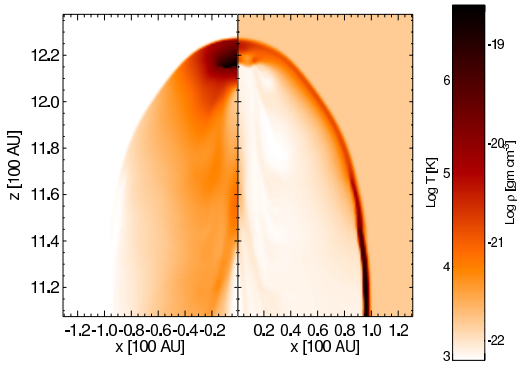

Figure 3. An enlargement of the post shock region in a linear grey scale: temperature on the left, density on the right.

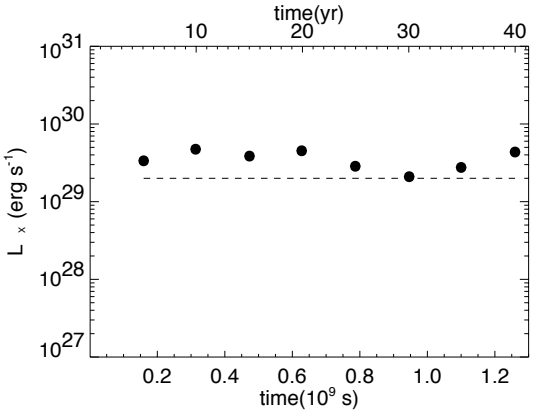

Figure 4. Evolution of the X-ray luminosity (dots; adapted from Bonito et al. 2004). The level of the X-ray luminosity derived from Raga et al. (2002) is marked as an horizontal dashed line.

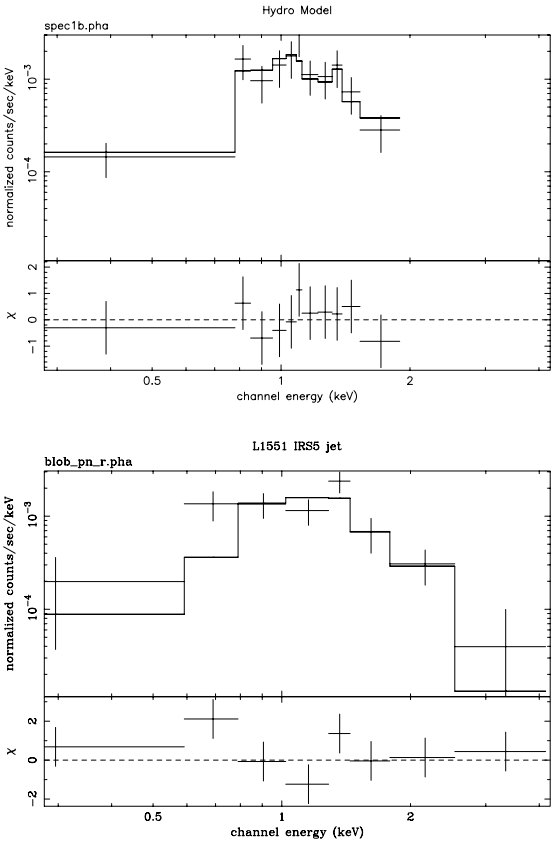

Figure 5. Upper panel: synthesized spectrum 25 years since the beginning of the jet-ambient interaction. The MEKAL best fitting spectrum is superimposed. Lower panel: observed EPIC-pn X-ray spectrum of the source HH 154 (Favata et al. 2002).

Table 1. Best-fit parameters to the EPIC-pn simulated X-ray spectrum derived from the hydrodynamic model (shown in Fig. 5) and to the EPIC-pn data analyzed by Favata et al. (2002).

	Hydro model	Favata et al.
count rate (cnts/ks)	1.2	1.0
D (pc)	150	150
$N_{\rm H}$ (10^{22} cm^{-2})	1.5 ± 0.3	1.4 ± 0.4
T (10^6 K)	3.4 ± 1.2	4.0 ± 2.5
$F_{\rm X}$ (10^{-13} erg/cm^2/s)	1.4	1.3

nates from the hot and dense blob localized just behind the shock front (Fig. 3). In addition our model allows us to predict a detectable proper motion for the X-ray blob and a slight variability of the X-ray luminosity which fluctuates of ±40% over the 40 yr modeled.

From observations of HH 154 (Fig. 1, Bally et al. 2003) the X-ray detection is very close to the originating star. Two different scenarios based on our model can explain a X-ray emission source so close to the protostar. First, such an emission could be due to the interaction of the jet with a circumstellar cloud localized close to the protostar. This is plausible considering the strong inhomogeneity of the interstellar medium in the star forming region from which the protostellar jet originates. Alternatively, assuming a pulsed jet instead of a continuous one, and noting that our model predicts that the X-ray emission is detectable since the beginning of the interaction between the protostellar jet and the ambient medium, the X-ray source observed in HH 154 may be explained as the emission due to the shock formed at the jet/ambient front at the beginning of the interaction. Bally et al. (2003) proposed that the

X-ray emission may be due to X-rays scattered from the protostellar coronae itself; such a mechanism, causing X-ray coming from the initial jet collimation, would show no proper motion. Our model unambiguously predicts a detectable proper motion of the X-ray source. In order to discriminate among the various proposed models, we proposed a new *Chandra* observation (approved in AO6) of HH 154 which will allow us to study the X-ray emitting region and its proper motion. From the analysis of new XMM-*Newton* data, we will compare the $L_{\rm X}$ variability (if any) with that obtained from our simulations.

Acknowledgements

The software used in this work was in part developed by the DOE-supported ASCI/Alliances Center for Astrophysical Thermonuclear Flashes at the University of Chicago, using modules for thermal conduction and optically thin radiation constructed at the Osservatorio Astronomico di Palermo. The calculations were performed on the Compaq cluster at the SCAN (Sistema di Calcolo per l'Astrofisica Numerica) facility of the INAF – Osservatorio Astronomico di Palermo "G.S. Vaiana" and on the IBM/Sp4 machine at CINECA (Bologna, Italy). This work was supported in part by Ministero dell'Istruzione, dell'Università e della Ricerca (MIUR) and by Istituto Nazionale di Astrofisica (INAF).

References

Bally, J., Feigelson, E., Reipurth, B. 2003, ApJ, 584, 843
Bonito, R., Orlando, S., Peres, G. et al. 2004, A&A, 424, L1
Bonito, R., Orlando, S., Peres, G. et al. 2005, in preparation
Cowie, L., McKee, C., 1977, ApJ, 35, 419 ApJ, 211, 135
Dalton, W., Balbus, S., 1993 ApJ, 404, 625
Favata, F., Fridlund, M., Micela, G. 2002, A&A, 386, 204
Fridlund, M., Liseau, R. 1998, ApJ, 499, L75
Fryxell, B., Olson, K., Ricker, P. et al. 2000, ApJ, 131, 273
Haro, G. 1953, ApJ, 117, 73
Herbig, G. 1950, ApJ, 111, 11
MacNeice, P., Olson, K., Mobarry, C. et al. 2000, Computer Physics Comm., 126, 330
Mewe, R., Gronenschild, E., van der Oord, G. et al. 1985, A&A, 62, 197
Morrison, R., McCammon, D. 1983, ApJ, 270, 119
Orlando, S., Peres, G., Reale, F. et al. 2000, ApJ, 528, 524
Pravdo, S., Feigelson, E., Garmire, G. et al. 2001, Nat, 413, 708
Pravdo, S., Tsuboi, Y., Maeda, Y. et al. 2004, ApJ, 605, 259
Raga, A., Noriega-Crespo, A., Velazquez, P. et al. 2002, ApJ, 576, L149
Raymond, J., Smith, B., 1977, ApJ, 35, 419
Spitzer, L., 1962, Physics of Fully Ionized Gases, New York: Interscience, 1962
Tsujimoto, M., Koyama, K., Kobayashi, N. et al. 2004, PASJ, 56, 341